Prediction of plant diversity in grasslands using Sentinel-1 and -2 satellite image time series

Mathieu Fauvel, Mailys Lopes, Titouan Dubo, Justine Rivers-Moore,
Pierre-Louis Frison, Nicolas Gross, Annie Ouin

Prediction of plant diversity in grasslands using Sentinel-1 and -2 satellite image time series

Mathieu Fauvel[a,*], Mailys Lopes[b], Titouan Dubo[b], Justine Rivers-Moore[b], Pierre-Louis Frison[d], Nicolas Gross[c], Annie Ouin[b]

[a]CESBIO, Université de Toulouse, CNES/CNRS/INRA/IRD/UPS, Toulouse, France
[b]DYNAFOR, Université de Toulouse, INRA, Castanet-Tolosan, France
[c]UCA, INRA, VetAgro Sup, UMR 0874 Ecosystème Prairial, 63000 Clermont-Ferrand, France
[d]LaSTIG, Université Paris-Est, IGN, 5 Bd Descartes, Champs sur Marne,77455 Marne la Vallée, France

Abstract

The prediction of grasslands plant diversity using satellite image time series is considered in this article. Fifteen months of freely available Sentinel optical and radar data were used to predict taxonomic and functional diversity at the pixel scale (10m×10m) over a large geographical extent ($40\,000\,\mathrm{km}^2$). 415 field measurements were collected in 83 grasslands to train and validate several statistical learning methods. The objective was to link the satellite spectro-temporal data to the plant diversity indices. Among the several diversity indices tested, Simpson and Shannon indices were best predicted with a coefficient of determination around 0.4 using a Random Forest predictor and Sentinel-2 data. The use of Sentinel-1 data was not found to improve significantly the prediction accuracy. Using the Random Forest algorithm and the Sentinel-2 time series, the prediction of the Simpson index was performed. The resulting map highlights the intra-parcel variability and demonstrates the capacity of satellite image time series to monitor grasslands plant taxonomic diversity from an ecological viewpoint.

Keywords: Satellite image time series, Sentinel-1&-2, Statistical learning, Grasslands, taxonomic diversity

1. Introduction

Natural and semi-natural grasslands cover 22% of the European agricultural land surface (Bengtsson et al., 2019). Grasslands are today one of the most endangered ecosystems due to land use change, agricultural intensification, and abandonment (Pärtel et al., 2005). Grasslands host a unique biodiversity, which support the provision of key ecosystem services such as carbon storage, food production crop polination, pest regulation and contribute to landscape scale amenities such as landscape scenic view. Permanent grasslands are crucial to maintain biodiversity in many agricultral landscape (Watkinson and Ormerod, 2001; Habel et al., 2013), and particularly insect diversity: they provide host plants, nectar, pollen (Ockinger and Smith, 2007) as well as nest sites (Carrié et al., 2018; Potts and Willmer, 1997).

Yet, despite recent regulation in favor of grasslands, agriculture intensification, abandonment and urbanization generate a decrease of both grasslands surface area and plant diversity (O'Mara, 2012; Newbold et al., 2016) leading to a loss of biodiversity (plants, insects, birds) and its related ecosystem services. Therefore, there is an urgent need to monitor grasslands over large extents in order to assess their current state in terms of area covered but also to estimate their plant diversity and their carrying capacity for insect populations. While the area information can be extracted from land cover databases (e.g. CORINE Land Cover (Heymann, 1994)) diversity and carrying capacity data are scarcely available. Though, spatial location, extent and quality of grasslands are crucial for their conservation per se but also to produce maps of related ecosystem services in agricultural areas. For instance, *mobile agents based ecosystem services* (Kremen et al., 2007) such as pollination and pest regulation rely on the presence of a mosaic of crops and semi-natural elements among which grasslands are crucial and represent the largest surface area.

Plant diversity is usually assessed by botanical surveys of the grasslands and indices related to the diversity in species of a community are commonly computed (richness, Shannon and Simpson diversity (Magurran, 2004)). Functional diversity can also be derived from the botanical survey through *functional types*, i.e., set of species exhibiting similar attributes having similar effect on ecosystems (Diaz and Cabido, 2001). Field surveys, sometimes called ground-truth in the remote sensing community, require

---

*Corresponding author
Email addresses: mathieu.fauvel@inra.fr (Mathieu Fauvel), mailys.lopes@inra.fr (Mailys Lopes), titouan-dubo@hotmail.fr (Titouan Dubo), justine.rivers-moore@inra.fr (Justine Rivers-Moore), pierre-louis.frison@univ-mlv.fr (Pierre-Louis Frison), nicolas.gross@inra.fr (Nicolas Gross), annie.ouin@ensat.fr (Annie Ouin)

significant human and material resources, the knowledge of the assessor and a sampling strategy, which make them expensive and time consuming (Magurran, 2004). Ecological surveys are thus limited in spatial extent and in temporal frequency, limiting grassland monitoring to a local scale and usually over a short period of time. Although field surveys provide valuable and high quality data at a point scale, they cannot easily be upscaled while taking into account the landsape heterogeneity. Therefore, field surveys alone cannot address the needs to monitor grassland biodiversity over large spatial extents and other techniques relating to field surveys should be considered.

Among such complementary techniques, remote sensing has received an increasing attention in the last decades (Turner, 2014; Buck et al., 2015). However, grasslands have been rarely studied in the remote sensing literature compared to other land covers like crops or forest (Newton et al., 2009). Most of the studies focusing on grasslands have agronomic applications, such as estimating biomass productivity and growth rate (Gu and Wylie, 2015; Li et al., 2013) or deriving biophysical parameters like the *Leaf Ara Index* (LAI), the *fraction of Photosynthetically Active Radiation* (fPAR) or the *fraction of Vegetation Cover* (fCOVER) (Darvishzadeh et al., 2008; He et al., 2009).

Regarding ecological applications, Corbane et al. (2013) mapped semi-natural grasslands types using two RapidEye images, while Stenzel et al. (2017) used five RapidEye images to classify high nature value grasslands. Species richness of herbaceous ecosystems such as grasslands, prairies and savannah was assessed using airborne hyperspectral imagery in Möckel et al. (2016), Gholizadeh et al. (2019) and Oldeland et al. (2010), respectively. Airborne hyperspectral imagery has also been used to map groups of species (Schuster et al., 2015), flower types (Landmann et al., 2015) or pollination types (Feilhauer et al., 2016).

Schematically, the different approaches to analyse grassland with remote sensing data can be divided into three categories: 1. Techniques that use vegetation indices or spectral reflectance as explanatory variables (Rapinel et al., 2019; Féret et al., 2015) 2. Techniques that use the spatial heterogeneity of vegetation indices as explanatory variables (Goodin and Henebry, 1998; Tuanmu and Jetz, 2015), 3. Techniques that use the "spectral variation hypothesis" (SVH) to extract explanatory variables (Lopes et al., 2017b; Hall et al., 2012).

In terms of remote sensing data, the majority of the studies having ecological schemes were conducted using very high spatial resolution data (≤ 5 meters/pixel), *e.g.*, hyperspectral data issued from an airborne sensor or multispectral satellite data such as RapidEye. Although a very high spatial resolution might seem necessary to estimate grasslands plant diversity as plant are typically small in grasslands, these types of acquisitions are limited in time and in space because of their current cost. In addition, medium spatial resolution satellite image time series (*e.g*, MODIS or SPOT-VEGETATION) have been found not appropriate for small and heterogeneous elements, such as grasslands. In particular, Ali et al. (2016) have stated that the moderate spatial resolution "*precludes their use for field-scale application in many countries*". As a consequence, the grassland biodiversity monitoring from remote sensing data is nowadays limited to "*low temporal resolution & small spatial cover & high spatial resolution*" (Giménez et al., 2017; Wang et al., 2019; Gholizadeh et al., 2019; Lopatin et al., 2017) or "*high temporal resolution & large spatial cover & coarse spatial resolution*" (Ge et al., 2018; Schmidt et al., 2018; Yang et al., 2018; Barrett et al., 2014; Si et al., 2012).

The launch of Sentinel-1&-2 satellites, issued from the European Union Copernicus and European Space Agency program, has enabled continuous and regular monitoring of small vegetated areas over large spatial extents thanks to their high spatial resolution (10m per pixel) and their frequent revisit (every 5 days for Sentinel-2) (Drusch et al., 2012; Defourny et al., 2019). Sentinel-1&-2 satellite image time series (SITS) open new possibilities to bridge the gap between high spatial resolution and high temporal resolution. First, their high temporal resolution enables the monitoring of plant phenology. Because plant communities differ in their temporal behavior, the phenological diversity measured by these sensors could be used as a proxy to estimate the plant diversity. Second, they provide complementary information about the grassland cover: optical data are influenced by chemical composition of the elements while radar data are sensitive to the geometric configuration of the elements (Joshi et al., 2016). Then, being available for free, they can be used to process large areas and complement field surveys at a reduced cost. Yet, recent works using Sentinel-2 images are still performed on small areas (a few square kilometers) (Rapinel et al., 2019). Although interesting, studies over such small areas do not have to cope with a high diversity of grasslands in terms of composition neither with the spatial variability of meteorological, topographical conditions and farmers pratices. Hence, it is unlikely that classification accuracies reported in such cases can be reached on larger spatial areas. Furthermore, they do not cope with the spectro-temporal variability of Sentinel satellite image series.

In this paper, we use Sentinel's optical and radar SITS to estimate plant taxonomic and functional diversity in grasslands over a a large spatial extent ($40\,000\,\text{km}^2$) for one growing season. Fifteen months of acquisitions of Sentinel-1&-2 images were used to predict at the pixel level plant diversity indices (richness, Shannon and Simpson diversity indices) and functional diversity indices related to pollination (flower diversity, insect dependence) of grasslands located in farmed landscapes in the southwest of France. Various linear and non-linear algorithms were investigated to cover different kinds of possible statistical relationships between the biodiversity indices and the SITS.
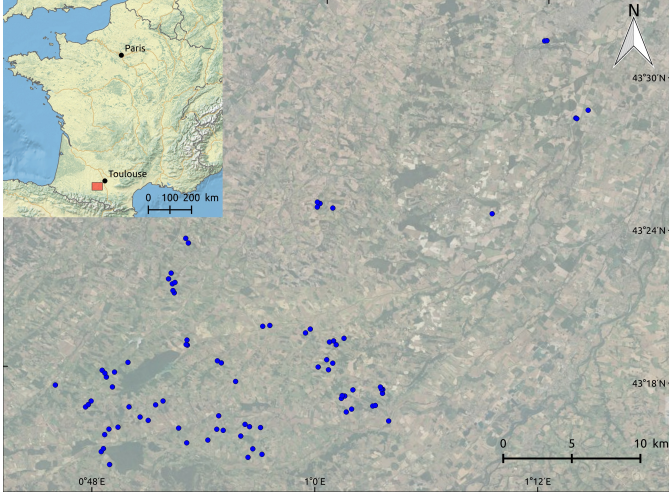
Figure 1: Study area. The region in the black frame is a zoom of the red area at the bottom of the image. The blue circles indicate the sampled plots in the grasslands. See section 2.2 for a full description. Data: 1:10m Natural Earth I (https://www.naturalearthdata.com); BD ORTHO® 50 cm IGN (background aerial photography)

2. Materials

2.1. Study site

The study area is part of the Long-Term Socio-Ecological Research site "Pyrénées-Garonne" located in southwest France near the city of Toulouse (43 °17 0 N, 0 °54 0 E), see Figure 1. This hilly area of around 900 km² is characterized by a mosaic of crops, small woods and grasslands. It is dominated by mixed crop-livestock farming. Grasslands provide food for cattle by grazing and/or producing hay or silage. They range from mono-specific, annual grasslands sown with rye-grass (improved with mineral fertilizing and mown up to three times a year) to permanent, semi-natural grasslands composed of spontaneous plant species (not fertilized and mown once a year). Grasslands are mainly located on steep slopes, whereas annual crops are in the valleys on the most productive, often irrigated lands. The climate is sub-Atlantic with sub-Mediterranean and mountain influences (mean annual temperature, 12.5 °C; mean annual precipitation, 750 mm).

2.2. Field botanical surveys
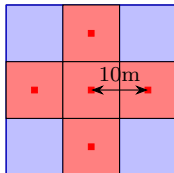
Figure 2: Field sampling: a plot (light red area) is made of 5 quadrats (red squares), 4 of them being located at 10 m from the center one. The light blue squares represent the corresponding Sentinel-2 pixel grid.

Table 1: Plant cover percentage bins.

Coverage estimation (%)	Assigned value (%)
[1, 2.5]	1
[2.5, 7.5]	5
[7.5, 11.5]	10
[11.5, 20]	15
[21, 30]	25
[31, 40]	35
[41, 50]	45
[51, 60]	55
[61, 70]	65
[71, 80]	75
[81, 90]	85
[91, 99]	95
100	100

Botanical surveys were conducted in 83 plots from distinct grasslands between April and May 2018 after the flowering and before the mowing. The average distance between two plots was 13.4 km with a standard deviation of 9.1 km and the minimum and the maximum distances were 0.08 km and 44.37 km, respectively. Each plot was composed of 5 quadrats of 1 square meter area (Figure 2). The center of each quadrat corresponded to the theoretical center of a Sentinel-2 pixel. Note that since the absolute geolocation is below 11 meter at 95.5% confidence (ESA, 2019), a possible mis-registration between Sentinel-2 data and GNSS can be observed for few pixels at some dates. After a ground checking and getting owners agreement, the position of the central quadrat was controlled with a high-accuracy GNSS handhelds (Trimble Geo 7X TerraSync). The grasslands were digitized using the agricultural Land Parcel Information System "Registre Parcellaire Graphique" (RPG) (Cantelaube and Carles, 2014).

Plants were identified at the species level and the abundance of each species was estimated by its cover percentage value in the one square meter area, according to 12 bins, see Table 1. Vegetation height was measured in two locations in each quadrat and averaged. A total of 415 quadrats (leading to 415 Sentinel pixels), belonging to 83 grasslands, was recorded and used in this study.

Three indices were computed using vegan package of R 3.2.3 (Oksanen et al., 2007; Team, 2012): plant richness S_q, defined as the number of plant species in quadrat q, the Shannon diversity index

$$H'(q) = -\sum_{s=1}^{S_q} p_{qs} \ln(p_{qs}),$$

where p_{qs} is the relative abundance of the species s in quadrat q and Simpson index of diversity (refers to Simpson index in the paper for simplicity) ,

$$L(q) = 1 - \sum_{s=1}^{S_q} p_{qs}^2.$$

The Shannon index measures heterogeneity taking into account the number of species and the relative abundance of

each species, while the Simpson index is the inverse of a dominance index reflecting how much the community is dominated (or not) by few species.

We also consider vegetation attribute related to pollination. Following Clough et al. (2014), Insect Dependence was assessed for each plant species, based on pollination syndrome (insects, wind, water..) and its frequency. The values were: **1** if insects are the major pollination vector, **0.5** if insects and an other vector are the major pollination vector, **0** if insects are not an important pollination vector. The Reward Index combines the amount of nectar and pollen which values run from: **0** for "none", **1** for "little", **2** for "present", **3** for "plenty". The sum of nectar and the amount of pollen score lead to values from 0 to 6 for the Reward Index of the species. Averaged at the community level using the FD package Laliberté and Legendre (2010) of R 3.2.3, the diversity and the abundance of these two vegetation attributes may reflect how species impact community and ecosystems. Finally, the Color Diversity was derived from the Shannon index,

$$CD(q) = -\sum_{j=1}^{J_q} r_{qj} \ln(r_{qj}),$$

where r_{qj} is the sum of the relative abundance of the species whom major color of flowers is j in quadrat q and J_q is the number of major colors in quadrat q.

The correlation matrix between the biodiversity indices is reported in Figure 3. Figure A.11 in Appendix A shows the distribution of indices for all the samples.
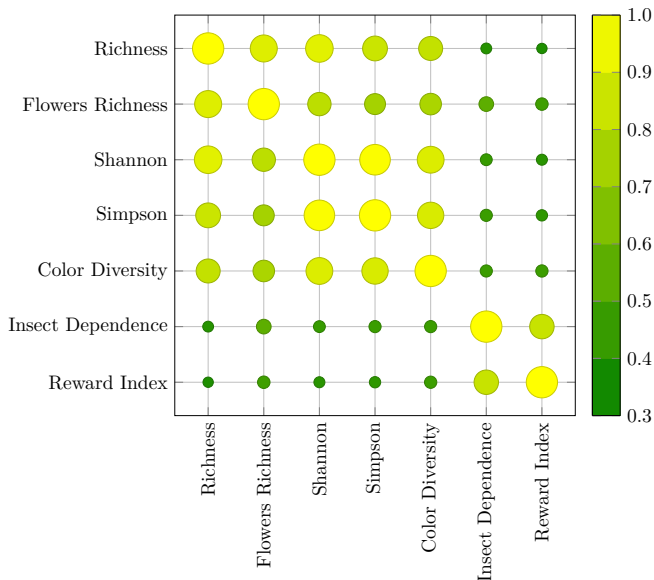
Figure 3: Correlation matrix of the biodiversity variables using the Spearman's rank correlation coefficient.

2.3. Satellite data

Both the optical and radar data were processed using the `iota`[2] software (Inglada et al., 2016), built on the *OrfeoToolbox* (OTB Development Team, 2018).

2.3.1. Optical data

Four Sentinel-2 tiles of Level 2A were downloaded from the Theia Land Data Centre[1], corresponding to all available acquisitions between August 26, 2017 and December 03, 2018[2]. Only the bands natively at 10 m/pixel were used in the experiments (blue, green, red and near-infrared). Surface reflectance time series were produced using the MAJA (*Multi-sensor atmospheric correction and cloud screening-ATCOR Joint Algorithm*) processing chain developed by the CNES-CESBIO and DLR. It includes orthorectification, atmospheric correction, clouds and shadows detection (Baetens et al., 2019). All the acquisitions were re-sampled and gap-filled (to handle clouds and shadows) onto the same set of dates (every 10 days, starting from 2017-08-29 and ending in 2018-12-02), as proceeded in Inglada et al. (2015). The final SITS contains 47 dates, in the visible and near infrared bands, corresponding to a total of 188 spectro-temporal features. The normalized difference vegetation index (NDVI) and the first principal components, accounting for 99% of the total variance, were extracted as alternative features (Tupin et al., 2014).

Figure 4 presents the reconstructed NDVI (in black) of the five quadrats for four plots as well as their corresponding detected shadows and clouds.

2.3.2. Radar data

Sentinel-1 Level-1 GRD (Ground Range Detected) time series recorded in interferometric wide swath mode were used. Four orbits corresponding to the Sentinel-2 extent were downloaded from the French Sentinel collaborative ground segment[3], corresponding to the same temporal period as Sentinel-2 time series. GRD time series were calibrated to γ^0, orthorectified and filtered using a multi-temporal spatial filter (Quegan and Yu, 2001). The parameters of the spatio-temporal filter were a spatial window of size 5×5 pixels and all the dates were used for the temporal filters. VV and VH polarizations were processed as well as the ratio VV/VH. The features were re-sampled onto the same set of dates (every 10 dates starting from 2017-08-27 to 2018-11-30).

Figure 4 presents the reconstructed γ^0(VV) polarization (in blue) for descending orbits for the same four plots.

3. Methods

For this work, a set of radiometric features commonly used with optical and radar data is investigated. Table 2 shows the various combinations of features used in the regression algorithms[4].

---

[1]http://www.theia-land.fr/en/presentation/products

[2]Images tagged as composed of more than 90% of cloudy pixels by the MAJA processing chain are not processed by the data center.

[3]https://peps.cnes.fr/rocket/#/home

[4]Dynamic habitat indices, such as in Hobi et al. (2017), as well as VV/VH ascending/descending features alone were tested, but the results were too bad and are not reported in the paper for the sake of clarity.

Table 2: List of inputs used for the prediction. The last column provides the number of variables for each input.

Acronym	Description	Size
S2	Blue, Green, Red and Near Infra-red spectral bands for all temporal acquisitions.	188
NDVI	NDVI for all the temporal acquisitions.	47
S2 NDVI	Combination of S2 and NDVI.	235
S2 PCA	First principal component accounting for 99% of the cumulative variance computed on S2.	49
R IR	Red and Near Infra-red spectral bands for all temporal acquisitions.	94
S1	VV, VH and ratio for all temporal acquisitions.	279
S1 S2	Full stack of S1 and S2 data.	467
PCA S1 S2	First principal component accounting for 99% of the cumulative variance computed on the S1 and S2 stack.	117
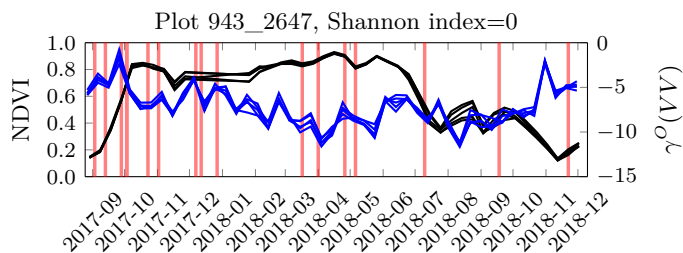
Figure 4: Reconstructed S2-NDVI (in black) and S1-VV polarization (in blue) with a 10 days step for different plots. For each plot, the 5 pixels corresponding to each quadrat are plotted. The red vertical lines indicate the dates of the detected clouds and shadows for the raw S2 pixels, before the gap-filling.

3.1. Regression techniques

Five conventional machine learning algorithms were used in the experiments with different set-up (Lary et al., 2016): Linear regression (with ridge and lasso regularization) (Hastie et al., 2009, Chap. 3), K-Nearest Neighbors (K-NN) (Hastie et al., 2009, Chap. 13), Kernel Ridge Regression (KRR) (Murphy, 2013, Chap. 14), Random Forest (RF) (Hastie et al., 2009, Chap. 15) and Gaussian Process (GP) (Rasmussen and Williams, 2006). K-NN, KRR, RF and GP are non-parametric and non-linear algorithms that have been used successfully in many remote sensing applications, see for instance Maxwell et al. (2018). In all the experiments, the Scikit-learn python library was used (Pedregosa et al., 2011). Hyperparameters of ridge, lasso, K-NN, RF and KR methods were fitted through cross-validation (Hastie et al., 2009, Chap 7) and those for GP were found by maximizing of the likelihood (Rasmussen and Williams, 2006).

3.2. Statistical accuracy assessment

The accuracy of the prediction of a biodiversity variable value y was assessed using the *coefficient of determination* (r^2) (Draper and Smith, 1998):

$$r^2 = 1 - \frac{\sum_{i=1}^{n_v}(y_i - \hat{y}_i)^2}{\sum_{i=1}^{n_v}(y_i - \bar{y})^2}$$

where n_v is the number of validation sample, y_i is the true biodiversity variable value associated with the ith sample, $\hat{y}_i$ is its corresponding predicted value and $\bar{y}$ is the mean value of the validation sample.

In order to correctly estimate r^2, the *k-fold cross validation* was used. Cross-validation directly estimates the *generalization error* of a given method (Hastie et al., 2009, Chap. 7): The data is split into K almost equal-size folds, and the model is fitted on $K - 1$ folds. The prediction error, here r^2, is computed on the remaining unseen fold. This process is done for all folds $k = 1, 2, \ldots, K$. The average error over the K folds is the estimated generalization error.
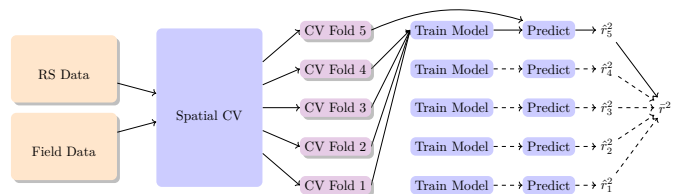
Figure 5: Spatial cross validation processing flow. For clarity, only the data assignment between the folds and the training step for the estimation of $\hat{r}_5^2$ is shown. This process is performed for every biodiversity variable.

However, in our experimental setting, the 5 quadrats corresponding to one plot are spatially correlated and this must be taken into account when constructing the K folds of the cross-validation (Hammond and Verbyla, 1996). It is proposed in this work to perform a grouped cross validation by splitting the samples according to their plot membership (Pohjankukka et al., 2017; Le Rest et al., 2014): quadrats from a same plot are all included in one fold and not shared among several folds. Hence, in the experiments, a five fold-grouped cross validation was performed, where the first four folds contain 16 plots (80 quadrats) and the last fold contains 19 plots (95 quadrats). The same splits were used for all experiments, i.e., the error assessment was done using the same folds whatever the methods, data sources and indices. Figure 5 shows the whole process.

Table 3: Estimated accuracy for the best predicted variables ($\hat{r}^2 > 0.3$) and the corresponding standard deviation ($\hat{\sigma}_{r^2}$) of the 5-fold spatial cross validation.

Data	Variable	Method	$\hat{r}^2$	$\hat{\sigma}_{r^2}$
R IR	Simpson	RF	0.45	0.13
R IR	Shannon	RF	0.43	0.13
S2	Color Diversity	RF	0.40	0.08
S1 S2	Richness	KRidge	0.34	0.15
S1 S2	Insect Dependence	KRidge	0.32	0.15
S1 S2	Flowers Richness	KRidge	0.32	0.16
S1 S2	Reward Index	GP RBF	0.32	0.20

4. Results

The Appendix C shows the results for the prediction of each variable. For clarity, only the best results for each variable corresponding to an average $\hat{r}^2 > 0.3$ are presented in the core of the paper, Table 3.
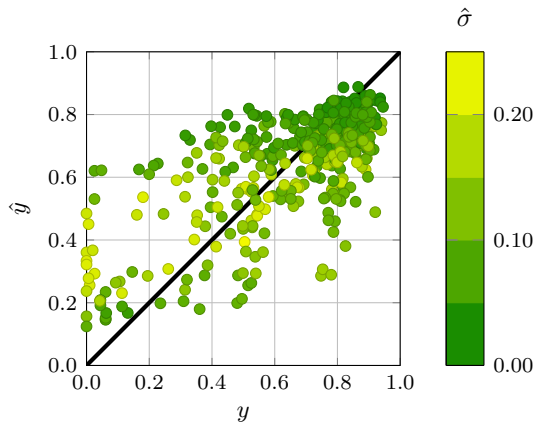
Figure 6: Scatter plot of the predicted Simpson values obtained with RF and R-IR data (see table 3). The black line is the identity line, i. e., when $\hat{y} = y$; $\hat{r}^2 = 0.45$. The colormap corresponds to the confidence interval $\hat{\sigma}$ of the prediction.

4.1. Biodiversity indices prediction accuracy

Of all indices, four indices were predicted with an estimated $\hat{r}^2$ above 0.3 and three indices above 0.4. The best predictions are obtained for the taxonomic diversity indices, i.e., Richness, Shannon and Simpson. These indices are strongly correlated (Figure 3), but they are also correlated with Color Diversity, which is well predicted too. The two others indices, Insect Dependence and Reward Index are not correlated with the others ones and are less accurately predicted.

The scatter plot of the prediction for the best result is displayed in Figure 6, and the second and third best results are displayed in Appendix B, figures B.12 and B.13. They were built during the spatial cross validation. They also show the confidence interval of the Random Forest predictions for each plot (see the colormap). Their main tendency is that lower values of indices is overestimated (above the black line) while high values are underestimated (below the black line).

4.2. Impact of the regression algorithm

Linear method with ridge regularization performs the worst in terms of prediction accuracy. Lasso and K-NN provide in-between results, sometimes Lasso works better, e.g., for Shannon, sometimes K-NN works better, e.g., for Simpson and sometimes they perform equally bad than the other methods. Among linear models, Lasso provides the best results, but it does not reach the best accuracy and the corresponding estimated $\hat{r}^2$ are usually low. Non linear regression methods, such as RF, GP and kernel ridge, provide overwhelmingly the best results.

From Table 3, RF is the method that provides the best overall results for three indices with an estimated $\hat{r}^2$ above 0.4. Kernel methods follow closely. Gaussian process performs slightly better on average than Kernel ridge. Regarding the influence of the kernel used in the GP, no significant differences are observed. For instance, Shannon indices were predicted with a $\hat{r}^2$ of 0.39±0.20 for the Rational quadratic kernel and of 0.38±0.19 for the RBF kernel, see Table C.6.

From the different results, no best method clearly appears. Depending on the indices, they may perform almost equally well for some indices while for others indices one method clearly outperforms the other ones. For instance, for Richness in table C.4, the estimated highest $\hat{r}^2$ are 0.32 for the GP with a rational quadratic kernel and 0.34 for the Kernel Ridge with a RBF kernel. However, for Simpson (table C.7), RF provides the best prediction by far with a $\hat{r}^2$ of 0.45 while GP RBF and GP RQ reach only 0.31.

4.3. Influence of the data source

From the tables in Appendix C, the optical data alone leads in general to better results than the radar data alone, see as example the Color Diversity results. Radar features did not lead to results close to the optical ones, for indices predicted with an $\hat{r}^2$ significantly higher than 0.

For the optical features, the NDVI and the PCA features are less informative than the original set of spectro-temporal features and the prediction accuracy is in general lower. However, combining the NDVI and spectro-temporal features can improve the prediction performance marginally for some indices, as it can be seen for Shannon index, table C.6. Surprisingly, using only the red and infrared bands – those used to compute the NDVI – results in highest, or close to highest, accuracy for most of the biodiversity indices, see for instance in Table 3.

Combining optical and radar data has positive influence on the prediction accuracy for some indices. For instance in Table 3, the four last indices were best predicted using a full stack of S1 and S2 features. Again, applying PCA does not lead to an increase of the prediction accuracy.

4.4. Influence of the spatial auto-correlation

For the three best estimated indices, the prediction accuracy was also estimated using a conventional cross-

validation, *i.e.*, allowing plots to be split into several folds. Figure 7 shows the prediction accuracy with and without the spatial auto-correlation. It is clear from the results that the quality of the prediction is overestimated when spatial auto-correlation is not taken into account. For instance for the Simpson index, the estimated $\hat{r}^2$ is approximately 35% lower when the spatial cross-validation is used.
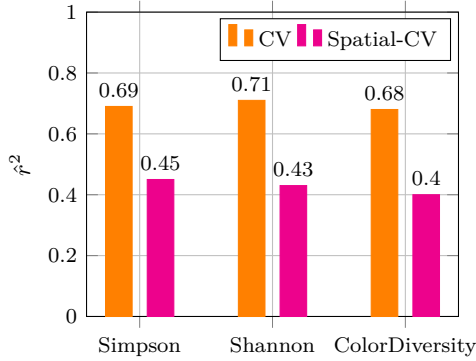
Figure 7: Influence of the spatial auto-correlation on the estimation of the prediction accuracy. "*Spatial-CV*" indicates that the spatial auto-correlation was taken into account during the fold construction of the cross validation, see section 3.2 for details.

4.5. Large scale map

Prediction of the *Simpson* index at the pixel level was done for all the grassland parcels identified from the Land Parcel Information System (RPG) over the four Sentinel-2 tiles with the data and method that resulted in the highest prediction accuracy (i.e., R-IR satellite data and RF algorithm, see Table 3). The confidence interval was also computed. Figure 8 shows an extract of the predicted Simpson value in a square of 1 km^2 centered on the plot 10_470. It also shows a very high spatial resolution aerial image from 2016 over the same extent as well as the confidence interval associated with the prediction of the Simpson index obtained with the Random Forest. Extracts for all plots are provided in the supplementary materials.

From the prediction, spatial heterogeneity in terms of Simpson value (and its associated confidence value) can be seen in the parcel, corresponding to intra-parcel heterogeneity of species distribution that can be captured with a spatial resolution of 10m/pixel. Furthermore, inter-parcel variability can be observed, even for adjacent fields.

The distribution of the predicted Simpson values over the entire area is reported in Figure 9 for the most representative types of grasslands identified on the RPG (i.e., *fallows, permanent grassland, long rotation meadow, temporary grassland, pastoral surface*). These types accounted for approximately 80% of the total grasslands area of the four tiles. The distribution of the Simpson index values exhibit strong differences w.r.t the grassland classes. For instance, *permanent grassland*, *long rotation meadow* and

temporary grassland have in average the highest values while *young fallow* and *pastoral surface* have the lowest values. Interestingly, *young* and *old fallow* present significant differences in terms of distribution, *young fallow* having lower Simpson indices (i.e., lower plant diversity) than *old fallow*.

5. Discussion

By using dense S2 and S1 SITS, this work contributed to the remote sensing of grasslands biodiversity using new generation high resolution SITS. It follows the works of Féret et al. (2015) and Rapinel et al. (2019) but rather than performing classification of grasslands types, the prediction of biodiversity indices and plant traits was considered as in Wang et al. (2019). Our study differed from the previously cited works by two important points. First, the area considered in our study site is much larger and thus accounts for more variability in the indices and in the remote sensing data, making the statistical learning problem more difficult but more realistic. Second, the spatial auto-correlation was taken into account when estimating the prediction error but leads to a lowest value (and rather more correct, i.e., less biased) of the prediction accuracy (Le Rest et al., 2014).

5.1. Prediction performance for biodiversity indices

Prediction of diversity measures were more accurate for diversity indices (Simpson and Shannon) than for species richness indices (e.g. Richness) as found in Oldeland et al. (2010). The Simpson index gives more weight to species with higher proportions while the richness is only based on species presence/absence. The presence of rare species (about 1% of cover) in the under storey will influence species richness but would be hardly detected by Sentinel sensor while dominant species are more detectable. Dominance indices such as Simpson are thus more indicated to estimate plant diversity with remote sensors. Functional diversity measures (Color Diversity, Insect Dependence and Reward Indices) showed a $\hat{r}^2$ above 0.3, which is promising as their link to optical or radar signal are less clear than species diversity. Even if flower cover never exceeds 20% of the grassland area, it may have been detected by the satellite sensors. Temporal variability of the signal may be linked to the different phenophase (period of flowering) in the grasslands. The link between diversity indices functionally related to pollination and satellite signals is truly interesting and opens new research frontiers. In particular, the prediction of land carrying capacity for pollinators at large extent based on actual relation between signal and functionality rather than expertise on suitability for pollinators based on satellite derived land cover is of most interest.

The spatial resolution of Sentinel images (10m×10m per pixel) might be too coarse to capture fine variation of plant composition. Gholizadeh et al. (2019) showed a loss
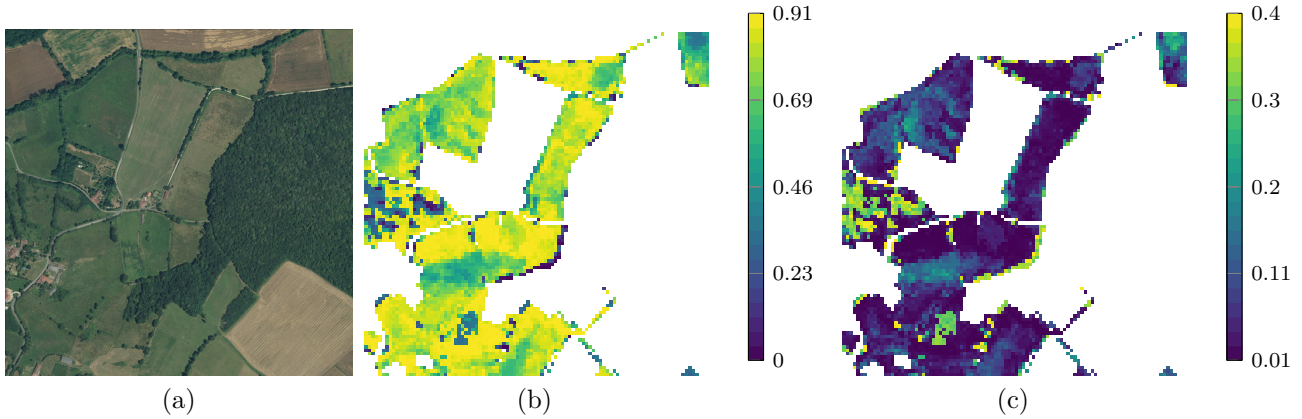
Figure 8: Simpson index around plot 132_1699. (a) Very high spatial resolution aerial image from 2016, (b) Prediction of the Simpson value for pixels corresponding to grasslands in the national agricultural Land Parcel Information System and (c) Confidence interval value associated to the prediction.
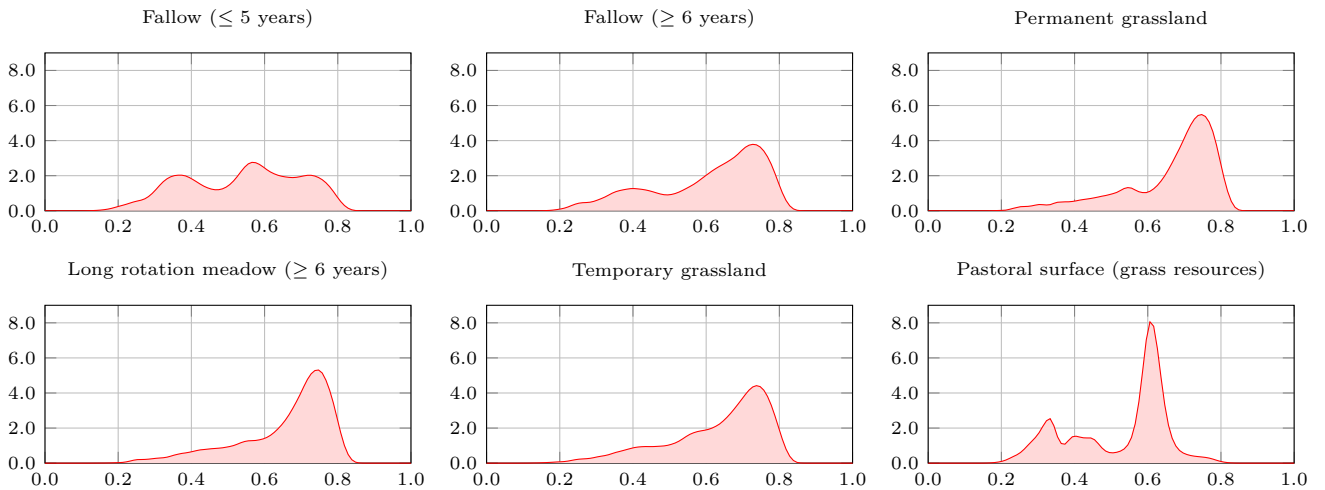
Figure 9: Distribution of the predicted Simpson index for the most represented types of grasslands identified from the RPG. The horizontal axis represents the Simpson index and the vertical axis represents the probability density function value associated with the Simpson index value. For the *fallow* classes or *long rotation meadow*, number in brackets indicates their ages. For the *pastoral surfaces*, the string in brackets indicates the most predominant resources in the parcels. The densities have been estimated by a non-parametric kernel density estimator with a Gaussian kernel and using the Scott rules for the selection of the bandwidth (Scott, 1992).

of correlation between the spectral feature and α-diversity index (Shannon) for simulated hyperspectral image with a spatial resolution above 2m per pixel. Nonetheless, they used only one date and captured little information about phenology. Feilhauer et al. (2013) found that spectral coverage of the entire solar-reflective domain is the most important characteristic to successfully assess floristic variation in grasslands, while multi-seasonal data did not improve it. These results obtained from simulated data contradict ours obtained with satellite imagery where the best prediction accuracies were reached using only the red and infrared bands and SITS. Our prediction accuracies are equivalent to the ones of Möckel et al. (2016) in predicting the inverse Simpson index in grasslands using airborne hyperspectral data. Their approach based on spectral reflectance reached a $\hat{r}^2$ of 0.45 using 245 wavebands and 0.40 using 35 wavebands. Our results suggest that dif-

ferences in phenology can be used as a proxy for plant diversity when spatial resolution and spectral resolution are not high enough.

Similar ideas were considered by Rapinel et al. (2019) who assumed that differences in phenology can be accounted for using SITS. However, in large scale setting, clouds and shadows are unavoidably present in the optical images, particularly during the key period for plant flowering (April-June), resulting in missing values that are reconstructed during the pre-processing. Figure 10 shows the proportion of masked pixels corresponding to the 415 quadrats: for the period between 2018-05-21 and 2018-06-20, the information was missing because of a too high level of clouds proportion (see section 2.3.1) and thus the corresponding dates were interpolated (Inglada et al., 2015). Hence, differences in terms of phenology during that period of time were not captured by the optical sensors and

could explain why the indices based on flower composition only were not accurately predicted. This also suggests that other drivers influencing the botanical composition are captured by the optical SITS, such as agricultural practices (Moog et al., 2002).

By comparison with our previous works (Lopes et al., 2017a,b), in which biodiversity indices were surveyed at the field scale, here the sampling was done at the pixel scale, with a spatial match between the sensor acquisition and the field work. This sampling strategy has a clear positive influence on the predictive accuracy, since the estimated $\hat{r}^2$ for the Shannon index was no more than 0.17 in (Lopes et al., 2017a). The heterogeneity of grasslands, in particular semi-natural grasslands, can be high and thus the spatial measurement unit of botanical composition should match as much as possible the sensor's spatial resolution. These findings show that the remote sensing-based estimation of plant diversity in grasslands should be done at the pixel level and not at the field level.

5.2. SITS pre-processing

In very cloudy situations, SAR data, not affected by clouds, provide additional information that can help for prediction (Clerici et al., 2017). Indeed, the combination of Sentinel-1 and Sentinel-2 SITS improved the prediction accuracy for some indices, e.g. Richness and Insect Dependence, but not for all. Sentinel-1 data can complement Sentinel-2 information for the learning algorithm, but SAR SITS alone are not sufficient. SAR data has been shown to provide relevant information for grassland management practices monitoring and cutting practices in particular (Voormansik et al., 2016; Hill et al., 1999; Dusseux et al., 2012). Hence, although SAR data was obviously not expected to be sensitive to botanical composition, it could have been sensitive to biomass, providing information about variations in plant height that could be associated with variation in species. Yet, S1 data was not found correlated to plant height in this study. However, the aforementioned works were conducted on a reduced geographical area and the variability in SAR acquisitions, e.g. due to different orbit and incident angles, were negligible in comparison with our context. Another possible explanation could be the smoothing effect of the spatio-temporal filter that alters the spatial resolution of S1-SITS and thus reduces the sensibility of such filtered data. This suggests in future studies to investigate a more sophisticated pre-processing of Sentinel-1 for a joint use with Sentinel-2 data.

In this work, the full stack of temporal acquisition was used, and the irregular temporal acquisitions between various Sentinel tiles was handled using linear interpolation (Inglada et al., 2015). This leads to a large amount of features, as displayed in Table 2, that can complexify the statistical learning step. In such situation, it is common to reduce the dimensionality, i.e., the number of features used. In this work, a conventional principal component analysis was used but it resulted in a loss of prediction

accuracy. More advanced feature extraction have been investigated, such as partial least square or forward feature reduction, but they did not improve the prediction accuracy. As Rapinel et al. (2019), we found that using the full set of Sentinel-2 bands (restricted here to spectral bands natively at 10m per pixel) works well in most of cases. Yet, using only red and near-infra red channels, with all the temporal features, provided very good results too. It may indicate that ignoring the spectro/backscatter or temporal structure of the Sentinel SITS when performing the dimension reduction is not appropriate and that further investigation is needed to extract relevant information from the data without loosing significant details.
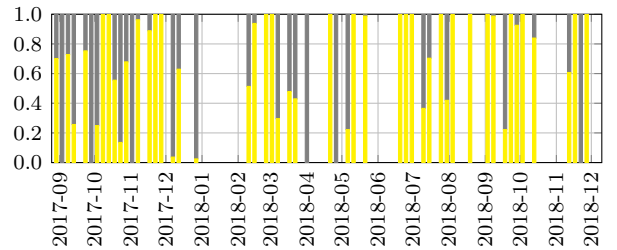
Figure 10: Proportion of free (in yellow) and masked (in gray) pixels for each temporal acquisition.

5.3. Importance of the spatial auto-correlation

Spatial auto-correlation was scarcely taken into account in previous studies on grasslands while it can have a strong influence on the estimated prediction accuracy (Hammond and Verbyla, 1996). Results obtained is this work are similar to those reported in Pohjankukka et al. (2017). This suggests that working on a large spatial area that allows the construction of a validation set that is spatially uncorrelated to the training set is an essential step to assess the quality of the results. Fortunately, with the increasing availability of high resolution SITS it will not be a critical issue in the future. However, for small spatial coverage data, such as hyperspectral or UAV ones, a careful statistical analysis should be done to prevent optimistic results.

5.4. Large scale prediction

The large scale map we produced highlights the grassland intra-parcel heterogeneity in terms of plant diversity, underlining the limits of predicting biodiversity indices at the field scale (Lopes et al., 2017b). Such a map can be used to assess the relationships between environmental factors and plant diversity at fine scale.

Part of the prediction associated with the large confidence interval observed in the images can be explained by geographical factors. First, the edges of the parcels could correspond to mixed pixels and therefore exhibit atypical values. Second, individual trees and hedgerows are sometimes included in the field. Their spectral-temporal features do not correspond to inputs from which the system is learned and unconfident predictions are done. Looking

9

at the confidence interval thus could inform on the reliability of the predicted values, at the pixel scale.

The decreasing average predicted Simpson values from the permanent, long rotation and temporary meadows observed on figure 9 are in accordance with the importance of long term no tillage and low intensity practices to keep grassland biodiversity at high level (Klimek et al., 2007). However, the temporary grasslands present a distribution of predicted Simpson values similar to the permanent ones. This pattern may be explained by the fact that the number of reported permanent grasslands by farmers is lower than the actual number (they are declared as "temporary" instead). This is because permanent grasslands have tillage restriction, while temporary grasslands do not. As a consequence, a large number of declared temporary grasslands are, actually, permanent grasslands.

5.5. Perspectives

Perspectives for this work are two-fold. First, field work for different grassland areas (mountains, wetland ...) should be conducted to enrich the learning database and to assess the robustness of the prediction at the country scale. Second, different stratification strategies should be investigated, for instance according to their types or their eco-climatic conditions. Third, additional data set, such as DEM or surface temperature, should be used jointly for the prediction in order to capture more information about grasslands. This would require specific methodological developments to properly use such a heterogeneous data set.

6. Conclusions

The prediction of grasslands biodiversity indices using Sentinel-1&-2 times series was investigated in this work. We have shown that abundance-based indices based on the dominance of some species (Simpson) can be predicted over a large area with a coefficient of determination above 0.4 using Sentinel-2 SITS.

This study indicates that the temporal information contained in the SITS can compensate for the limited spectral information and spatial resolution compared to hyperspectral imagery. Another finding is that the spatial autocorrelation tends to bias the estimation of the prediction accuracy and thus, should be taken into account during validation.

The contribution of this work does not lie in selecting the best set of dates nor the best machine learning regression methods but in assessing the potential of Sentinel-1 and -2 dense times series as explanatory variables for the prediction of grasslands biodiversity indices. We believe that our results, using large scale data with various agricultural practices for different meteorological and topographic conditions, demonstrate the capacity of such data to monitor grasslands from an ecological viewpoint. In particular, intra-parcel variability was highlighted in this work and can be monitored over large areas.

References

Ali, I., Cawkwell, F., Dwyer, E., Barrett, B., Green, S., 2016. Satellite remote sensing of grasslands: from observation to management. Journal of Plant Ecology 9, 649–671. URL: http://dx.doi.org/10.1093/jpe/rtw005, doi:10.1093/jpe/rtw005.

Baetens, L., Desjardins, C., Hagolle, O., 2019. Validation of copernicus sentinel-2 cloud masks obtained from maja, sen2cor, and fmask processors using reference cloud masks generated with a supervised active learning procedure. Remote Sensing 11. URL: http://www.mdpi.com/2072-4292/11/4/433, doi:10.3390/rs11040433.

Barrett, B., Nitze, I., Green, S., Cawkwell, F., 2014. Assessment of multi-temporal, multi-sensor radar and ancillary spatial data for grasslands monitoring in ireland using machine learning approaches. Remote Sensing of Environment 152, 109 – 124. URL: http://www.sciencedirect.com/science/article/pii/S0034425714002065, doi:https://doi.org/10.1016/j.rse.2014.05.018.

Bengtsson, J., Bullock, J.M., Egoh, B., Everson, C., Everson, T., O'Connor, T., O'Farrell, P.J., Smith, H.G., Lindborg, R., 2019. Grasslands—more important for ecosystem services than you might think. Ecosphere 10, e02582. URL: https://esajournals.onlinelibrary.wiley.com/doi/abs/10.1002/ecs2.2582, doi:10.1002/ecs2.2582, arXiv:https://esajournals.onlinelibrary.wiley.com/doi/pdf/10.1002/

Buck, O., Millán, V.E.G., Klink, A., Pakzad, K., 2015. Using information layers for mapping grassland habitat distribution at local to regional scales. International Journal of Applied Earth Observation and Geoinformation 37, 83 – 89. URL: http://www.sciencedirect.com/science/article/pii/S0303243414002359, doi:https://doi.org/10.1016/j.jag.2014.10.012. special Issue on Earth observation for habitat mapping and biodiversity monitoring.

Cantelaube, P., Carles, M., 2014. Le registre parcellaire graphique: des données géographiques pour décrire la couverture du sol agricole. Le Cahier des Techniques de lINRA,(N Spécial GéoExpé) , 58–64.

Carrié, R., Lopes, M., Ouin, A., Andrieu, E., 2018. Bee diversity in crop fields is influenced by remotely-sensed nesting resources in surrounding permanent grasslands. Ecological Indicators 90, 606–614.

Clerici, N., Calderón, C.A.V., Posada, J.M., 2017. Fusion of sentinel-1a and sentinel-2a data for land cover mapping: a case study in the lower magdalena region, colombia. Journal of Maps 13, 718–726. URL: https://doi.org/10.1080/17445647.2017.1372316, doi:10.1080/17445647.2017.1372316, arXiv:https://doi.org/10.1080/17445647.2017.1372316.

Clough, Y., Ekroos, J., Báldi, A., Batáry, P., Bommarco, R., Gross, N., Holzschuh, A., Hopfenmüller, S., Knop, E., Kuussaari, M., Lindborg, R., Marini, L., Öckinger, E., Potts, S.G., Pöyry, J., Roberts, S.P., Steffan-Dewenter, I., Smith, H.G., 2014.

Density of insect-pollinated grassland plants decreases with increasing surrounding land-use intensity. Ecology Letters 17, 1168–1177. URL: https://onlinelibrary.wiley.com/doi/abs/10.1111/ele.12325, doi:10.1111/ele.12325.

Corbane, C., Alleaume, S., Deshayes, M., 2013. Mapping natural habitats using remote sensing and sparse partial least square discriminant analysis. International Journal of Remote Sensing 34, 7625–7647. URL: https://doi.org/10.1080/01431161.2013.822603, doi:10.1080/01431161.2013.822603.

Darvishzadeh, R., Skidmore, A., Schlerf, M., Atzberger, C., Corsi, F., Cho, M., 2008. Lai and chlorophyll estimation for a heterogeneous grassland using hyperspectral measurements. ISPRS Journal of Photogrammetry and Remote Sensing 63, 409 – 426. URL: http://www.sciencedirect.com/science/article/pii/S0924271608000166, doi:https://doi.org/10.1016/j.isprsjprs.2008.01.001.

Defourny, P., Bontemps, S., Bellemans, N., Cara, C., Dedieu, G., Guzzonato, E., Hagolle, O., Inglada, J., Nicola, L., Rabaute, T., Savinaud, M., Udroiu, C., Valero, S., Bégué, A., Dejoux, J.F., Harti, A.E., Ezzahar, J., Kussul, N., Labbassi, K., Lebourgeois, V., Miao, Z., Newby, T., Nyamugama, A., Salh, N., Shelestov, A., Simonneaux, V., Traore, P.S., Traore, S.S., Koetz, B., 2019. Near real-time agriculture monitoring at national scale at parcel resolution: Performance assessment of the sen2-agri automated system in various cropping systems around the world. Remote Sensing of Environment 221, 551 – 568. doi:https://doi.org/10.1016/j.rse.2018.11.007.

Diaz, S., Cabido, M., 2001. Vive la difference: Plant functional diversity matters to ecosystem processes. Trends in Ecology & Evolution 16, 646 – 655. URL: http://www.sciencedirect.com/science/article/pii/S0169534701022832, doi:https://doi.org/10.1016/S0169-5347(01)02283-2.

Draper, N., Smith, H., 1998. Applied regression analysis. Number v. 1 in Wiley series in probability and statistics: Texts and references section, Wiley. URL: https://books.google.fr/books?id=8n8pAQAAMAAJ.

Drusch, M., Bello, U.D., Carlier, S., Colin, O., Fernandez, V., Gascon, F., Hoersch, B., Isola, C., Laberinti, P., Martimort, P., Meygret, A., Spoto, F., Sy, O., Marchese, F., Bargellini, P., 2012. Sentinel-2: ESA's optical high-resolution mission for GMES operational services. Remote Sensing of Environment 120, 25 – 36. doi:https://doi.org/10.1016/j.rse.2011.11.026. the Sentinel Missions - New Opportunities for Science.

Dusseux, P., Gong, X., Corpetti, T., L. Hubert-Moy, S.C., 2012. Contribution of radar images for grassland management identification, in: SPIE Remote Sensing. URL: https://doi.org/10.1117/12.974547, doi:10.1117/12.974547.

ESA, 2019. L1c data quality report. https://sentinel.esa.int/documents/247904/685211/Sentinel-2_L1C_Data_Quality_Report.

Feilhauer, H., Doktor, D., Schmidtlein, S., Skidmore, A.K., 2016. Mapping pollination types with remote sensing. Journal of Vegetation Science 27, 999–1011. URL: https://onlinelibrary.wiley.com/doi/abs/10.1111/jvs.12421, doi:10.1111/jvs.12421.

Feilhauer, H., Thonfeld, F., Faude, U., He, K.S., Rocchini, D., Schmidtlein, S., 2013. Assessing floristic composition with multispectral sensors—a comparison based on monotemporal and multiseasonal field spectra. International Journal of Applied Earth Observation and Geoinformation 21, 218 – 229. URL: http://www.sciencedirect.com/science/article/pii/S0303243412001936, doi:http://dx.doi.org/10.1016/j.jag.2012.09.002.

Féret, J., Corbane, C., Alleaume, S., 2015. Detecting the phenology and discriminating mediterranean natural habitats with multispectral sensors—an analysis based on multiseasonal field spectra. IEEE Journal of Selected Topics in Applied Earth Observations and Remote Sensing 8, 2294–2305. doi:10.1109/JSTARS.2015.2431320.

Ge, J., Meng, B., Liang, T., Feng, Q., Gao, J., Yang, S., Huang, X., Xie, H., 2018. Modeling alpine grassland cover based on modis data and support vector ma-

chine regression in the headwater region of the huanghe river, china. Remote Sensing of Environment 218, 162 – 173. URL: http://www.sciencedirect.com/science/article/pii/S0034425718304309, doi:https://doi.org/10.1016/j.rse.2018.09.019.

Gholizadeh, H., Gamon, J.A., Townsend, P.A., Zygielbaum, A.I., Helzer, C.J., Hmimina, G.Y., Yu, R., Moore, R.M., Schweiger, A.K., Cavender-Bares, J., 2019. Detecting prairie biodiversity with airborne remote sensing. Remote Sensing of Environment 221, 38 – 49. URL: http://www.sciencedirect.com/science/article/pii/S0034425718304991, doi:https://doi.org/10.1016/j.rse.2018.10.037.

Giménez, M.G., de Jong, R., Peruta, R.D., Keller, A., Schaepman, M.E., 2017. Determination of grassland use intensity based on multi-temporal remote sensing data and ecological indicators. Remote Sensing of Environment 198, 126 – 139. URL: http://www.sciencedirect.com/science/article/pii/S0034425717302638, doi:https://doi.org/10.1016/j.rse.2017.06.003.

Goodin, D.G., Henebry, G.M., 1998. Seasonality of finely-resolved spatial structure of ndvi and its component reflectances in tallgrass prairie. International Journal of Remote Sensing 19, 3213–3220. doi:10.1080/014311698214280.

Gu, Y., Wylie, B.K., 2015. Developing a 30-m grassland productivity estimation map for central nebraska using 250-m modis and 30-m landsat-8 observations. Remote Sensing of Environment 171, 291 – 298. URL: http://www.sciencedirect.com/science/article/pii/S0034425715301693, doi:https://doi.org/10.1016/j.rse.2015.10.018.

Habel, J.C., Dengler, J., Janišová, M., Török, P., Wellstein, C., Wiezik, M., 2013. European grassland ecosystems: threatened hotspots of biodiversity. Biodiversity and Conservation 22, 2131–2138. URL: https://doi.org/10.1007/s10531-013-0537-x, doi:10.1007/s10531-013-0537-x.

Hall, K., Reitalu, T., Sykes, M.T., Prentice, H.C., 2012. Spectral heterogeneity of quickbird satellite data is related to fine-scale plant species spatial turnover in semi-natural grasslands. Applied Vegetation Science 15, 145–157. URL: https://onlinelibrary.wiley.com/doi/abs/10.1111/j.1654-109X.2011.01143.x, doi:10.1111/j.1654-109X.2011.01143.x, arXiv:https://onlinelibrary.wiley.com/doi/pdf/10.1111/j.1654-109X.

Hammond, T.O., Verbyla, D.L., 1996. Optimistic bias in classification accuracy assessment. International Journal of Remote Sensing 17, 1261–1266. doi:10.1080/01431169608949085.

Hastie, T., Tibshirani, R., Friedman, J.H., 2009. The elements of statistical learning: data mining, inference, and prediction, 2nd Edition. Springer series in statistics, Springer. URL: http://www.worldcat.org/oclc/300478243.

He, Y., Guo, X., Wilmshurst, J.F., 2009. Reflectance measures of grassland biophysical structure. International Journal of Remote Sensing 30, 2509–2521. doi:10.1080/01431160802552751.

Heymann, Y., 1994. CORINE land cover: Technical guide. Office for Official Publ. of the Europ. Communities.

Hill, M.J., Donald, G.E., Vickery, P.J., 1999. Relating radar backscatter to biophysical properties of temperate perennial grassland. Remote Sensing of Environment 67, 15 – 31. URL: http://www.sciencedirect.com/science/article/pii/S0034425798000637, doi:https://doi.org/10.1016/S0034-4257(98)00063-7.

Hobi, M.L., Dubinin, M., Graham, C.H., Coops, N.C., Clayton, M.K., Pidgeon, A.M., Radeloff, V.C., 2017. A comparison of dynamic habitat indices derived from different modis products as predictors of avian species richness. Remote Sensing of Environment 195, 142 – 152. URL: http://www.sciencedirect.com/science/article/pii/S0034425717301682, doi:https://doi.org/10.1016/j.rse.2017.04.018.

Inglada, J., Arias, M., Tardy, B., Hagolle, O., Valero, S., Morin, D., Dedieu, G., Sepulcre, G., Bontemps, S., Defourny, P., Koetz, B., 2015. Assessment of an operational system for crop type map production using high temporal and spatial resolution satellite optical imagery. Remote Sensing 7, 12356–12379. URL: http:

//www.mdpi.com/2072-4292/7/9/12356, doi:10.3390/rs70912356.

Inglada, J., Vincent, A., Arias, M., Tardy, B., 2016. iota2-a25386. URL: https://doi.org/10.5281/zenodo.58150, doi:10.5281/zenodo.58150.

Joshi, N., Baumann, M., Ehammer, A., Fensholt, R., Grogan, K., Hostert, P., Jepsen, M.R., Kuemmerle, T., Meyfroidt, P., Mitchard, E.T.A., Reiche, J., Ryan, C.M., Waske, B., 2016. A review of the application of optical and radar remote sensing data fusion to land use mapping and monitoring. Remote Sensing 8. URL: http://www.mdpi.com/2072-4292/8/1/70, doi:10.3390/rs8010070.

Klimek, S., Richter gen. Kemmermann, A., Hofmann, M., Isselstein, J., 2007. Plant species richness and composition in managed grasslands: The relative importance of field management and environmental factors. Biological Conservation 134, 559–570.

Kremen, C., Williams, N.M., Aizen, M.A., Gemmill-Herren, B., LeBuhn, G., Minckley, Robert a nd Packer, L., Potts, S.G., Roulston, T., Stef fan Dewenter, I., Vázquez, D.P., Winfree, R., Adams, L., Crone, E.E., Greenleaf, S.S., Keitt, T.H., Klein, A.M., Regetz, J., Ricketts, T.H., 2007. Pollination and other ecosystem services produced by mobile organisms: a conceptual framework for the effects of land-use change. Ecology Letters 10, 299–314. URL: https://onlinelibrary.wiley.com/doi/abs/10.1111/j.1461-0248.2007.01018.x, doi:10.1111/j.1461-0248.2007.01018.x, arXiv:https://onlinelibrary.wiley.com/doi/pdf/10.1111/j.1461-0248.2007.01018.x.

Laliberté, E., Legendre, P., 2010. A distance-based framework for measuring functional diversity from mutliple traits. Ecology 91, 299–305. Ao2846ev.

Landmann, T., Piiroinen, R., Makori, D.M., Abdel-Rahman, E.M., Makau, S., Pellikka, P., Raina, S.K., 2015. Application of hyperspectral remote sensing for flower mapping in african savannas. Remote Sensing of Environment 166, 50 – 60. URL: http://www.sciencedirect.com/science/article/pii/S0034425715300353, doi:https://doi.org/10.1016/j.rse.2015.06.006.

Lary, D.J., Alavi, A.H., Gandomi, A.H., Walker, A.L., 2016. Machine learning in geosciences and remote sensing. Geoscience Frontiers 7, 3 – 10. URL: http://www.sciencedirect.com/science/article/pii/S1674987115000821, doi:https://doi.org/10.1016/j.gsf.2015.07.003. special Issue: Progress of Machine Learning in Geosciences.

Le Rest, K., Pinaud, D., Monestiez, P., Chadoeuf, J., Bretagnolle, V., 2014. Spatial leave-one-out cross-validation for variable selection in the presence of spatial autocorrelation. Global Ecology and Biogeography 23, 811–820. URL: https://onlinelibrary.wiley.com/doi/abs/10.1111/geb.12161, doi:10.1111/geb.12161, arXiv:https://onlinelibrary.wiley.com/doi/pdf/10.1111/geb.12161.

Li, Z., Huffman, T., McConkey, B., Townley-Smith, L., 2013. Monitoring and modeling spatial and temporal patterns of grassland dynamics using time-series modis ndvi with climate and stocking data. Remote Sensing of Environment 138, 232 – 244. URL: http://www.sciencedirect.com/science/article/pii/S0034425713002320, doi:https://doi.org/10.1016/j.rse.2013.07.020.

Lopatin, J., Fassnacht, F.E., Kattenborn, T., Schmidtlein, S., 2017. Mapping plant species in mixed grassland communities using close range imaging spectroscopy. Remote Sensing of Environment 201, 12 – 23. URL: http://www.sciencedirect.com/science/article/pii/S0034425717303966, doi:https://doi.org/10.1016/j.rse.2017.08.031.

Lopes, M., Fauvel, M., Ouin, A., Girard, S., 2017a. Potential of sentinel-2 and spot5 (take5) time series for the estimation of grasslands biodiversity indices, in: 2017 9th International Workshop on the Analysis of Multitemporal Remote Sensing Images (Multi-Temp), pp. 1–4. doi:10.1109/Multi-Temp.2017.8035206.

Lopes, M., Fauvel, M., Ouin, A., Girard, S., 2017b. Spectro-temporal heterogeneity measures from dense high spatial resolution satellite image time series: Application to grassland species diversity estimation. Remote Sensing 9. URL: http://www.mdpi.com/2072-4292/9/10/993, doi:10.3390/rs9100993.

Magurran, A., 2004. Measuring Biological Diversity. Wiley. URL: https://books.google.fr/books?id=tUqzLSUzXxcC.

Maxwell, A.E., Warner, T.A., Fang, F., 2018. Implementation of machine-learning classification in remote sensing: an applied review. International Journal of Remote Sensing 39, 2784–2817. URL: https://doi.org/10.1080/01431161.2018.1433343, doi:10.1080/01431161.2018.1433343.

Moog, D., Poschlod, P., Kahmen, S., Schreiber, K.F., 2002. Comparison of species composition between different grassland management treatments after 25 years. Applied Vegetation Science 5, 99–106. URL: https://onlinelibrary.wiley.com/doi/abs/10.1111/j.1654-109X.2002.tb00539.x, doi:10.1111/j.1654-109X.2002.tb00539.x.

Murphy, K.P., 2013. Machine learning : a probabilistic perspective. MIT Press, Cambridge, Mass. [u.a.].

Möckel, T., Dalmayne, J., Schmid, B.C., Prentice, H.C., Hall, K., 2016. Airborne hyperspectral data predict fine-scale plant species diversity in grazed dry grasslands. Remote Sensing 8. URL: http://www.mdpi.com/2072-4292/8/2/133, doi:10.3390/rs8020133.

Newbold, T., Hudson, L.N., Arnell, A.P., Contu, S., De Palma, A., Ferrier, S., Hill, S.L.L., Hoskins, A.J., Lysenko, I., Phillips, H.R.P., Burton, V.J., Chng, C.W.T., Emerson, S., Gao, D., Pask-Hale, G., Hutton, J., Jung, M., Sanchez-Ortiz, K., Simmons, B.I., Whitmee, S., Zhang, H., Scharlemann, J.P.W., Purvis, A., 2016. Has land use pushed terrestrial biodiversity beyond the planetary boundary? a global assessment. Science 353, 288–291. URL: https://science.sciencemag.org/content/353/6296/288, doi:10.1126/science.aaf2201, arXiv:https://science.sciencemag.org/content/353/6296/288.full.pdf.

Newton, A.C., Hill, R.A., Echeverría, C., Golicher, D., Benayas, J.M.R., Cayuela, L., Hinsley, S.A., 2009. Remote sensing and the future of landscape ecology. Progress in Physical Geography: Earth and Environment 33, 528–546. URL: https://doi.org/10.1177/0309133309346882, doi:10.1177/0309133309346882, arXiv:https://doi.org/10.1177/0309133309346882.

Ockinger, E., Smith, H.G., 2007. Semi-natural grasslands as population sources for pollinating insects in agricultural landscapes. Journal of Applied Ecology 44, 50–59. Ao1658ev.

Oksanen, J., Kindt, R., Legendre, P., O'Hara, B., Stevens, M.H.H., 2007. Vegan: Community ecology package.ordination methods, diversity analysis and other functions for community and vegetation ecologists.

Oldeland, J., Wesuls, D., Rocchini, D., Schmidt, M., Jürgens, N., 2010. Does using species abundance data improve estimates of species diversity from remotely sensed spectral heterogeneity? Ecological Indicators 10, 390 – 396. URL: http://www.sciencedirect.com/science/article/pii/S1470160X09001241, doi:https://doi.org/10.1016/j.ecolind.2009.07.012.

O'Mara, F., 2012. The role of grasslands in food security and climate change. Annals of Botany 110, 1263–1270. doi:10.1093/aob/mcs209.

OTB Development Team, 2018. Orfeo toolbox 6.6.0. URL: https://doi.org/10.5281/zenodo.1294917, doi:10.5281/zenodo.1294917.

Pärtel, M., Bruun, H., Sammul, M., 2005. Biodiversity in temperate european grasslands: origin and conservation., in: Grassland Science in Europe, Grassland Science in Europe. pp. 1–14. The information about affiliations in this record was updated in December 2015. The record was previously connected to the following departments: Plant Ecology and Systematics (Closed 2011) (011004000).

Pedregosa, F., Varoquaux, G., Gramfort, A., Michel, V., Thirion, B., Grisel, O., Blondel, M., Prettenhofer, P., Weiss, R., Dubourg, V., Vanderplas, J., Passos, A., Cournapeau, D., Brucher, M., Perrot, M., Duchesnay, E., 2011. Scikit-learn: Machine learning in Python. Journal of Machine Learning Research 12, 2825–2830.

Pohjankukka, J., Pahikkala, T., Nevalainen, P., Heikkonen, J., 2017. Estimating the prediction performance of spatial models via spatial k-fold cross validation. International Journal of Geographical Information Science 31, 2001–2019. doi:10.1080/13658816.2017.1346255.

Potts, S., Willmer, P., 1997. Abiotic and biotic factors influencing

nest-site selection by halictus rubicundus, a ground-nesting halictine bee. Ecological Entomology 22, 319–328. URL: https://onlinelibrary.wiley.com/doi/abs/10.1046/j.1365-2311.1997.00071.x, doi:10.1046/j.1365-2311.1997.00071.x, arXiv:https://onlinelibrary.wiley.com/doi/pdf/10.1046/j.1365-2311.1997.00071.x.

Quegan, S., Yu, J.J., 2001. Filtering of multichannel sar images. IEEE Transactions on Geoscience and Remote Sensing 39, 2373–2379. doi:10.1109/36.964973.

Rapinel, S., Mony, C., Lecoq, L., Clément, B., Thomas, A., Hubert-Moy, L., 2019. Evaluation of sentinel-2 time-series for mapping floodplain grassland plant communities. Remote Sensing of Environment 223, 115 – 129. URL: http://www.sciencedirect.com/science/article/pii/S0034425719300185, doi:https://doi.org/10.1016/j.rse.2019.01.018.

Rasmussen, C., Williams, C., 2006. Gaussian Processes for Machine Learning. Adaptive Computation and Machine Learning, MIT Press, Cambridge, MA, USA.

Schmidt, S., Alewell, C., Meusburger, K., 2018. Mapping spatio-temporal dynamics of the cover and management factor (c-factor) for grasslands in switzerland. Remote Sensing of Environment 211, 89 – 104. URL: http://www.sciencedirect.com/science/article/pii/S0034425718301536, doi:https://doi.org/10.1016/j.rse.2018.04.008.

Schuster, C., Schmidt, T., Conrad, C., Kleinschmit, B., Förster, M., 2015. Grassland habitat mapping by intra-annual time series analysis – comparison of rapideye and terrasar-x satellite data. International Journal of Applied Earth Observation and Geoinformation 34, 25 – 34. URL: http://www.sciencedirect.com/science/article/pii/S0303243414001378, doi:https://doi.org/10.1016/j.jag.2014.06.004.

Scott, D., 1992. Multivariate Density Estimation: Theory, Practice, and Visualization. A Wiley-interscience publication, Wiley. URL: https://books.google.fr/books?id=7crCUS_F2ocC.

Si, Y., Schlerf, M., Zurita-Milla, R., Skidmore, A., Wang, T., 2012. Mapping spatio-temporal variation of grassland quantity and quality using meris data and the prosail model. Remote Sensing of Environment 121, 415 – 425. URL: http://www.sciencedirect.com/science/article/pii/S0034425712001046, doi:https://doi.org/10.1016/j.rse.2012.02.011.

Stenzel, S., Fassnacht, F.E., Mack, B., Schmidtlein, S., 2017. Identification of high nature value grassland with remote sensing and minimal field data. Ecological Indicators 74, 28 – 38. URL: http://www.sciencedirect.com/science/article/pii/S1470160X16306422, doi:https://doi.org/10.1016/j.ecolind.2016.11.005.

Team, R.c., 2012. R: A language and environment for statistical computing.

Tuanmu, M.N., Jetz, W., 2015. A global, remote sensing-based characterization of terrestrial habitat heterogeneity for biodiversity and ecosystem modelling. Global Ecology and Biogeography 24, 1329–1339. URL: https://onlinelibrary.wiley.com/doi/abs/10.1111/geb.12365, doi:10.1111/geb.12365.

Tupin, F., Inglada, J., Nicolas, J., 2014. Remote Sensing Imagery. ISTE, Wiley. URL: https://books.google.fr/books?id=GfcXAwAAQBAJ.

Turner, W., 2014. Sensing biodiversity. Science 346, 301–302. URL: http://science.sciencemag.org/content/346/6207/301, doi:10.1126/science.1256014, arXiv:http://science.sciencemag.org/content/346/6207/301.full.pdf.

Voormansik, K., Jagdhuber, T., Zalite, K., Noorma, M., Hajnsek, I., 2016. Observations of cutting practices in agricultural grasslands using polarimetric sar. IEEE Journal of Selected Topics in Applied Earth Observations and Remote Sensing 9, 1382–1396. doi:10.1109/JSTARS.2015.2503773.

Wang, Z., Townsend, P.A., Schweiger, A.K., Couture, J.J., Singh, A., Hobbie, S.E., Cavender-Bares, J., 2019. Mapping foliar functional traits and their uncertainties across three years in a grassland experiment. Remote Sensing of Environment 221, 405 – 416. URL: http://www.sciencedirect.com/science/article/pii/S003442571830525X, doi:https://doi.org/10.1016/j.rse.2018.11.016.

Watkinson, A.R., Ormerod, S.J., 2001. Grasslands, grazing and biodiversity: editor's introduction. Journal of Applied Ecology 38, 233–237. doi:10.1046/j.1365-2664.2001.00621.x.

Yang, S., Feng, Q., Liang, T., Liu, B., Zhang, W., Xie, H., 2018. Modeling grassland above-ground biomass based on artificial neural network and remote sensing in the three-river headwaters region. Remote Sensing of Environment 204, 448 – 455. URL: http://www.sciencedirect.com/science/article/pii/S0034425717304741, doi:https://doi.org/10.1016/j.rse.2017.10.011.

Appendix A. Biodiversity indices distribution
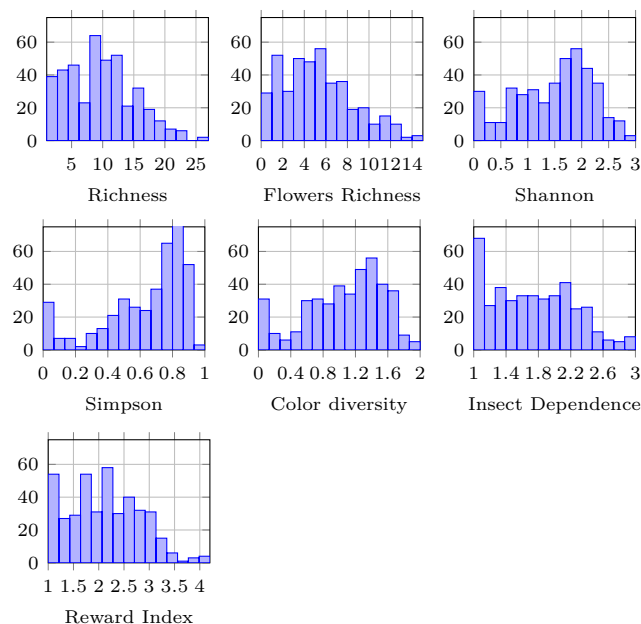
Figure A.11: Histogram of indices derived from the botanical survey.

Appendix B. Scatter plots

Appendix C. Average R2

Table C.4: Estimated $\bar{r}^2$ for Richness

	GP RBF	GP RQ	Ridge	Lasso	RF	KNN	KRidge
S2	0.17	0.26	-0.28	0.09	0.24	0.05	0.10
NDVI	0.03	0.21	-0.50	0.02	0.15	0.07	0.13
S2 NDVI	0.15	0.26	-0.29	0.06	0.20	0.03	0.06
S2 PCA	0.14	0.20	-0.71	0.13	0.09	0.11	0.19
PCA	0.13	0.27	-0.85	0.07	0.21	0.13	0.22
S1	0.24	0.28	-0.55	0.17	0.11	0.08	0.22
S1 S2	0.30	0.32	-0.25	0.09	0.27	0.12	0.34
PCA S1 S2	0.12	0.21	-1.11	0.14	0.20	0.12	0.21
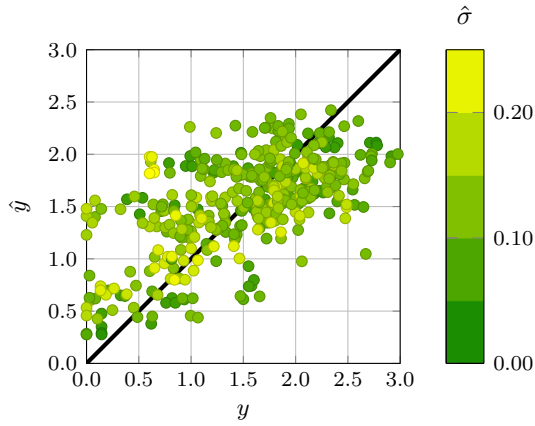
Figure B.12: Scatter plot of the predicted Shannon values obtained with RF and R-IR data (see table 3). The black line is the identity line, i. e., when $\hat{y} = y$; $\hat{r}^2 = 0.43$. The colormap corresponds to the confidence interval $\hat{\sigma}$ of the prediction.
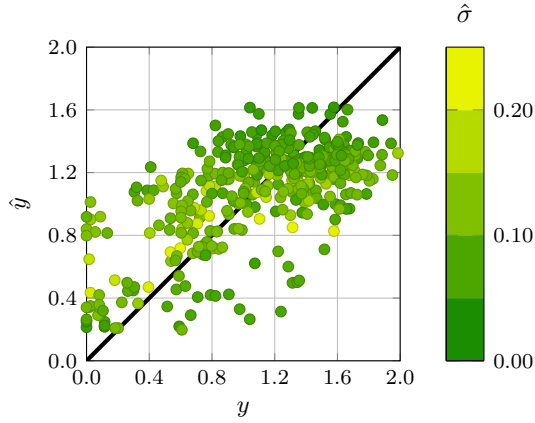
Figure B.13: Scatter plot of the predicted color diversity values obtained with RF and S2 data (see table 3). The black line is the identity line $\hat{y} = y$; $\hat{r}^2 = 0.40$. The colormap corresponds to the confidence interval $\hat{\sigma}$ of the prediction.

Table C.7: Estimated $\bar{r}^2$ for Simpson

	GP RBF	GP RQ	Ridge	Lasso	RF	KNN	KRidge
S2	0.29	0.27	-0.24	-0.12	0.44	0.16	0.10
NDVI	0.19	0.26	-0.16	0.13	0.30	0.20	0.07
S2 NDVI	0.27	0.25	-0.13	-0.01	0.43	0.18	0.12
S2 PCA	0.16	0.20	-0.52	0.19	0.25	0.25	0.01
R IR	0.27	0.27	-0.57	-0.12	0.45	0.24	0.08
S1	0.26	0.26	-0.48	-0.11	0.15	0.16	0.14
S1 S2	0.31	0.31	-0.36	-0.04	0.41	0.23	0.19
PCA S1 S2	0.20	0.22	-0.88	0.22	0.03	0.20	0.09

Table C.8: Estimated $\bar{r}^2$ for Color Diversity

	GP RBF	GP RQ	Ridge	Lasso	RF	KNN	KRidge
S2	0.29	0.28	-0.24	-0.06	0.40	0.13	0.22
NDVI	0.17	0.26	-0.23	-0.02	0.25	0.13	0.12
S2 NDVI	0.27	0.27	-0.18	0.03	0.34	0.16	0.23
S2 PCA	0.13	0.19	-0.40	0.17	0.26	0.18	0.05
R IR	0.27	0.28	-0.31	0.02	0.39	0.20	0.16
S1	0.23	0.22	-0.74	0.01	0.14	0.13	0.23
S1 S2	0.33	0.33	-0.47	0.11	0.35	0.16	0.30
PCA S1 S2	0.14	0.20	-0.54	0.25	0.06	0.16	0.09

Table C.9: Estimated $\bar{r}^2$ for Insect Dependence

	GP RBF	GP RQ	Ridge	Lasso	RF	KNN	KRidge
S2	0.11	0.18	-0.21	0.25	0.27	0.17	0.29
NDVI	0.04	0.20	0.03	0.24	0.18	0.21	0.24
S2 NDVI	0.12	0.19	-0.24	0.26	0.25	0.19	0.29
S2 PCA	0.04	0.07	-0.35	0.12	0.07	0.09	0.14
R IR	0.12	0.18	-0.17	0.23	0.22	0.17	0.28
S1	0.14	0.15	-0.26	0.11	0.08	-0.03	0.18
S1 S2	0.29	0.30	-0.39	0.28	0.25	0.18	0.32
PCA S1 S2	0.02	0.09	-0.51	0.19	0.09	0.11	0.22

Table C.5: Estimated $\bar{r}^2$ for Flowers Richness

	GP RBF	GP RQ	Ridge	Lasso	RF	KNN	KRidge
S2	0.12	0.19	-0.35	0.08	0.16	0.02	0.09
NDVI	0.02	0.16	-0.37	-0.05	0.15	0.02	0.07
S2 NDVI	0.09	0.19	-0.43	0.09	0.17	0.01	0.09
S2 PCA	0.10	0.15	-0.71	0.07	0.10	0.07	0.10
R IR	0.08	0.20	-0.62	0.06	0.11	0.03	0.13
S1	0.21	0.25	-0.62	0.22	0.15	0.09	0.21
S1 S2	0.28	0.30	-0.42	0.12	0.23	0.08	0.32
PCA S1 S2	0.06	0.14	-1.04	0.09	0.06	0.07	0.05

Table C.6: Estimated $\bar{r}^2$ for Shannon

	GP RBF	GP RQ	Ridge	Lasso	RF	KNN	KRidge
S2	0.30	0.31	-0.08	0.06	0.40	0.13	0.16
NDVI	0.17	0.31	-0.21	0.05	0.24	0.18	0.22
S2 NDVI	0.28	0.30	-0.00	0.13	0.41	0.15	0.17
S2 PCA	0.20	0.26	-0.30	0.29	0.28	0.21	0.26
R IR	0.28	0.35	-0.43	0.11	0.43	0.23	0.18
S1	0.31	0.32	-0.27	0.20	0.14	0.19	0.25
S1 S2	0.38	0.39	-0.08	0.21	0.34	0.15	0.31
PCA S1 S2	0.22	0.28	-0.61	0.29	0.24	0.23	0.18

Table C.10: Estimated $\bar{r}^2$ for Reward Indice

	GP RBF	GP RQ	Ridge	Lasso	RF	KNN	KRidge
S2	0.15	0.24	-0.12	0.24	0.23	0.15	0.27
NDVI	0.07	0.24	-0.11	0.23	0.24	0.23	0.23
S2 NDVI	0.14	0.24	-0.17	0.24	0.22	0.15	0.30
S2 PCA	0.08	0.15	-0.31	0.18	0.09	0.06	0.15
R IR	0.14	0.23	-0.09	0.25	0.24	0.15	0.22
S1	0.12	0.12	-0.62	0.09	0.12	0.00	0.17
S1 S2	0.32	0.32	-0.56	0.25	0.26	0.16	0.29
PCA S1 S2	0.06	0.17	-0.45	0.21	0.11	0.09	0.25